ARTICLES

A contractile nuclear actin network drives chromosome congression in oocytes

Péter Lénárt[1]†, Christian P. Bacher[2], Nathalie Daigle[1], Arthur R. Hand[3], Roland Eils[2], Mark Terasaki[4,5] & Jan Ellenberg[1]

Chromosome capture by microtubules is widely accepted as the universal mechanism of spindle assembly in dividing cells. However, the observed length of spindle microtubules and computer simulations of spindle assembly predict that chromosome capture is efficient in small cells, but may fail in cells with large nuclear volumes such as animal oocytes. Here we investigate chromosome congression during the first meiotic division in starfish oocytes. We show that microtubules are not sufficient for capturing chromosomes. Instead, chromosome congression requires actin polymerization. After nuclear envelope breakdown, we observe the formation of a filamentous actin mesh in the nuclear region, and find that contraction of this network delivers chromosomes to the microtubule spindle. We show that this mechanism is essential for preventing chromosome loss and aneuploidy of the egg—a leading cause of pregnancy loss and birth defects in humans.

In dividing eukaryotic cells, microtubules are believed to be involved in all aspects of spindle assembly[1]. In prophase, long interphase microtubules depolymerize[2,3] and centrosomes nucleate M-phase asters of short and dynamic microtubules. After nuclear envelope breakdown (NEBD), astral microtubules invade the nuclear region, 'search and capture' chromosomes and then align them on the spindle[4,5]. Rapid turnover of microtubules is essential for spindle assembly[5,6], but limits their maximal length to about 20 μm (refs 7, 8). Consequently, chromosome capture is inefficient at distances greater than 40 μm away from the centrosomes[9]. Chromosomes are not completely passive during this process but may facilitate capture by generating a high local concentration of RanGTP[10] and/or by directly nucleating microtubules on their surface[11]. Computer simulations have shown that with such bias towards chromosomes, 'search and capture' can indeed function in somatic cells at experimentally observed timescales[12]. However, the model also predicts microtubule capture to be inefficient in cells with nuclei larger than 30 μm in diameter[12].

Animal oocytes store large amounts of nuclear proteins and RNA for early embryonic divisions, and thus have much larger nuclei. Starfish oocytes are a typical example and are excellent specimens for live-cell confocal microscopy owing to their transparency and fast, reliable maturation. Oocytes arrested at meiotic prophase I are 170 μm in diameter and contain a large, 80-μm nucleus at the animal pole of the cell. Typically for oocytes, condensed chromosomes (1–2 μm in size) are randomly scattered across the nucleoplasm. The two centrosomes are located at the animal pole, sandwiched between the cell cortex and the nuclear envelope[13]. After addition of the maturation hormone 1-methyladenine, oocytes re-enter meiosis, leading to NEBD in 20 min (ref. 14). After NEBD, chromosomes move towards the centrosomes and form the first meiotic spindle under the cell cortex, 40 min after hormone addition. Extrusion of the first polar body 1 h after hormone treatment then completes meiosis I[13].

During meiosis I, chromosomes in the oocytes of starfish and many other animals have to travel much longer distances to the spindle than in somatic cells. Consequently, microtubule 'search and capture' is likely to be inefficient. Here we show that in starfish oocytes, chromosome congression is driven by a contractile actin network. This network forms and fills the nuclear region after NEBD, and by its contraction delivers the embedded chromosomes to within the ~30-μm capture range of microtubule asters. We show that this mechanism is essential, because actin-depolymerizing or stabilizing drugs cause chromosome loss and lead to the formation of aneuploid eggs.

Asters are too short to capture chromosomes

First, we analysed meiotic chromosome movement by imaging microtubules and chromosomes in live as well as in fixed oocytes during maturation, when chromosomes travel up to 80 μm to reach the meiotic spindle. Before NEBD, we visualized a large array of cytoplasmic microtubules anchoring the nucleus to the animal pole[15] (Fig. 1a, time −3:24 and Supplementary Video S1). These microtubules rapidly depolymerized at NEBD and centrosomes started to nucleate short M-phase asters (Fig. 1a, b) with a maximal length of 15–20 μm (Fig. 1c). Nevertheless, all chromosomes, including those more than 40 μm away from the closest microtubule end, moved towards the animal pole immediately after NEBD (Fig. 1c and Supplementary Video S1). This movement occurred 5–10 min before microtubules contacted those distal chromosomes, as visualized in live cells or by immunofluorescence (Fig. 1a–c), suggesting that a mechanism other than microtubule capture is responsible for chromosome congression in meiosis I. To test this directly, we depolymerized microtubules using nocodazole (Supplementary Fig. S1a). We found that chromosome congression proceeded almost normally in the absence of microtubules. All chromosomes gathered in a compact group under the cell cortex at the animal pole, as for untreated cells (Fig. 2a, b).

[1]Gene Expression and Cell Biology/Biophysics Programmes, European Molecular Biology Laboratory (EMBL), Meyerhofstrasse 1, D-69117 Heidelberg, Germany. [2]Theoretical Bioinformatics B080, German Cancer Research Center (DKFZ), Im Neuenheimer Feld 580, D-69120 Heidelberg, Germany. [3]Departments of Orthodontics, Oral and Maxillofacial Surgery, Pediatric Dentistry and Advanced General Dentistry, and [4]Department of Physiology, University of Connecticut Health Center, Farmington, Connecticut 06030, USA. [5]Marine Biological Laboratory, Woods Hole, Massachusetts 02543, USA. †Present address: Research Institute of Molecular Pathology (IMP), Dr Bohr-Gasse 7, A-1030 Vienna, Austria.

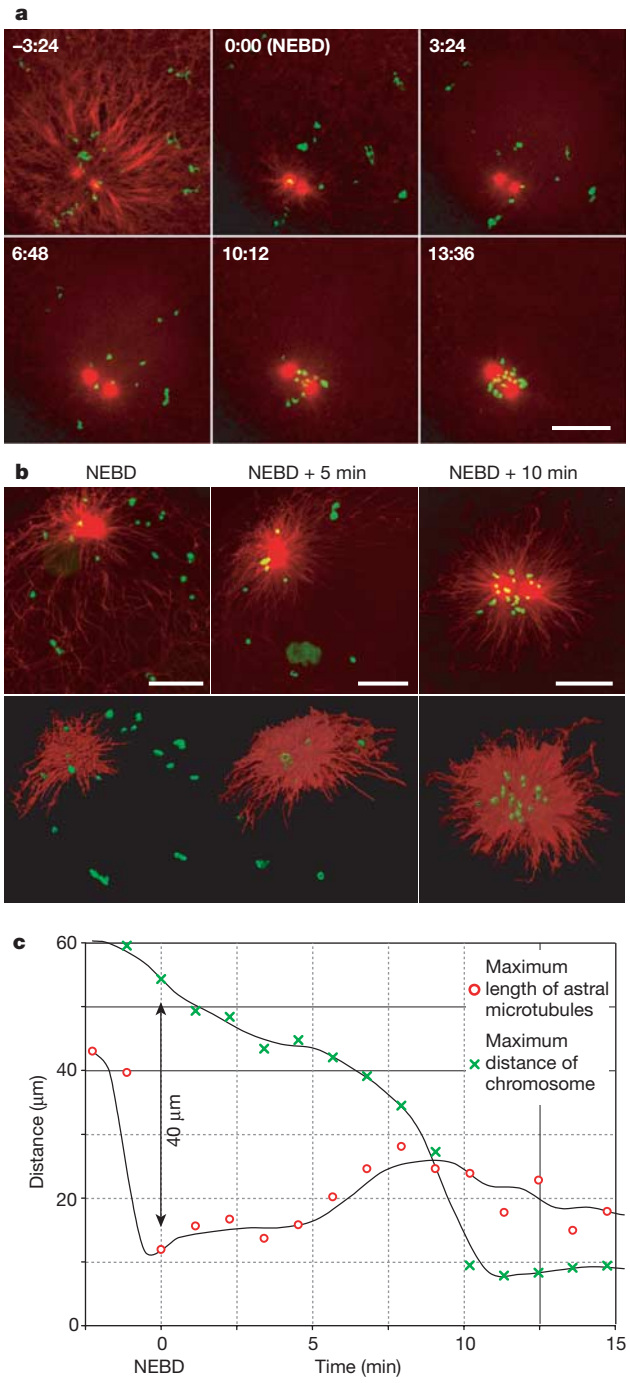

Figure 1 | Chromosomes congress without attachment to meiotic asters. **a**, 3D time-lapse (4D) imaging of a maturing oocyte expressing ensconsin–3EGFP (microtubules, red) and injected with Alexa-568-Ran (chromosomes, green) (20 sections every 4 μm, stacks of images taken every 68 s). Images show *Z*-projections of selected time points; a full series is shown in Supplementary Video S1. Time shown in minutes and seconds. Scale bar, 20 μm. **b**, Immunofluorescence of oocytes. *Z*-projections (top row) and isosurface reconstructions (bottom row). Microtubules shown in red, DNA in green. Scale bar, 20 μm. Residual interphase microtubules not connected to centrosomes, and nucleoli were removed in isosurface reconstructions. **c**, Quantification of data in **a**, showing the maximal distance of chromosomes from the midpoint between centrosomes (green crosses) and the maximal length of astral microtubules (red circles) over time. In fixed oocytes, microtubules 5–10 μm longer were occasionally found. Lines show running average fits.

Chromosome congression is actin-dependent

As microtubules were not required for long-range directional chromosome movement, we tested other cytoskeletal components for their involvement. Strikingly, when the actin cytoskeleton was disrupted during maturation by latrunculin B (Supplementary Fig. S1b), congression failed in 75% of the cells (Fig. 2a, b). It seems that only chromosomes close enough to centrosomes were captured by microtubules, while more distal chromosomes were lost (Fig. 2a). As chromosomes are positioned randomly in the nucleus, chromosomes in the remaining 25% of the cells were probably already in close proximity to the centrosomes before NEBD, and thus could all be captured by microtubules. To exclude the possibility that chromosomes in these oocytes congressed independently of both actin and microtubules, we also treated cells with a combination of nocodazole and latrunculin B. This caused complete failure of chromosome congression, and chromosomes remained scattered in the nuclear region in 100% of the cells (Fig. 2a, b).

To characterize congression defects caused by latrunculin B treatment, we quantified chromosome movement in live oocytes expressing histone H2B fused to a red fluorescent protein (H2B–diHcRed[16]). In three-dimensional time-lapse (4-dimensional) data sets, chromosomes were reconstructed by isosurface rendering and tracked (Fig. 2c, see Supplementary Videos S2–S5 for videos and reconstructions). In untreated cells, tracking revealed two distinct phases of movement. At NEBD, chromosomes started to move synchronously with a speed of $\sim 3\,\mu m\,min^{-1}$ in the general direction of the animal pole, as if connected to each other (Fig. 2d, e). Between 5 and 15 minutes after NEBD, when chromosomes entered the range of short astral microtubules 20–40 μm away from the animal pole, they individually switched to a faster speed ($>12\,\mu m\,min^{-1}$), changed direction and moved straight towards the centrosomes (arrows in Fig. 2d, e; Supplementary Video S2). Nocodazole completely prevented this second fast movement (Fig. 2d, e), which thus corresponds to chromosome capture by microtubules. In the absence of microtubules, chromosomes nevertheless continued to move at the slow speed, eventually reaching the animal pole (Fig. 2d, e and Supplementary Video S3), confirming our observations in fixed cells (Fig. 2a, b).

The initial slower phase of microtubule-independent chromosome movement was markedly affected by depolymerizing actin with latrunculin B. Long incubation periods with low doses (120 nM, which is still compatible with cell integrity) greatly decreased the initial movement (Supplementary Fig. S2). However, the residual motion was often sufficient to move chromosomes within 40 μm of the centrosomes and microtubules were still able to capture many chromosomes (Supplementary Video S9). Higher concentrations of latrunculin B (2 μM), which completely prevent actin polymerization, could be used if added just a few minutes before NEBD. This completely abolished movement of distal chromosomes (asterisks in Fig. 2d, e), which did not reach the animal pole even by the time the few proximal chromosomes that had been captured by microtubules entered anaphase (Supplementary Video S4). Despite chromosome loss, anaphase initiated without delay, indicating that the spindle checkpoint is easily bypassed or might not be active in meiosis I of starfish oocytes. Failure of the actin-dependent phase of chromosome congression thus led to formation of an aneuploid egg.

Treating oocytes with the combination of nocodazole and latrunculin B prevented any directional movement of chromosomes (Fig. 2d, e and Supplementary Video S5), demonstrating that microtubules and actin account for all chromosome dynamics observed in untreated cells. Results similar to those with latrunculin B were also obtained with 1 μM cytochalasin D (refs 17, 18 and data not shown).

NEBD triggers nuclear actin polymerization

We have shown that an actin-dependent mechanism is necessary for

delivering distal chromosomes to within the capture distance of centrosomal microtubules to prevent chromosome loss. To visualize the structures responsible for this actin-dependent congression in live oocytes we injected them with fluorescently labelled actin. Before NEBD, a significant fraction of fluorescent actin was localized to the nucleus, but we did not detect any nuclear actin structures (Fig. 3a) or observe staining of polymerized actin by phalloidin in nuclei of fixed cells (not shown). Additionally, before NEBD, actin

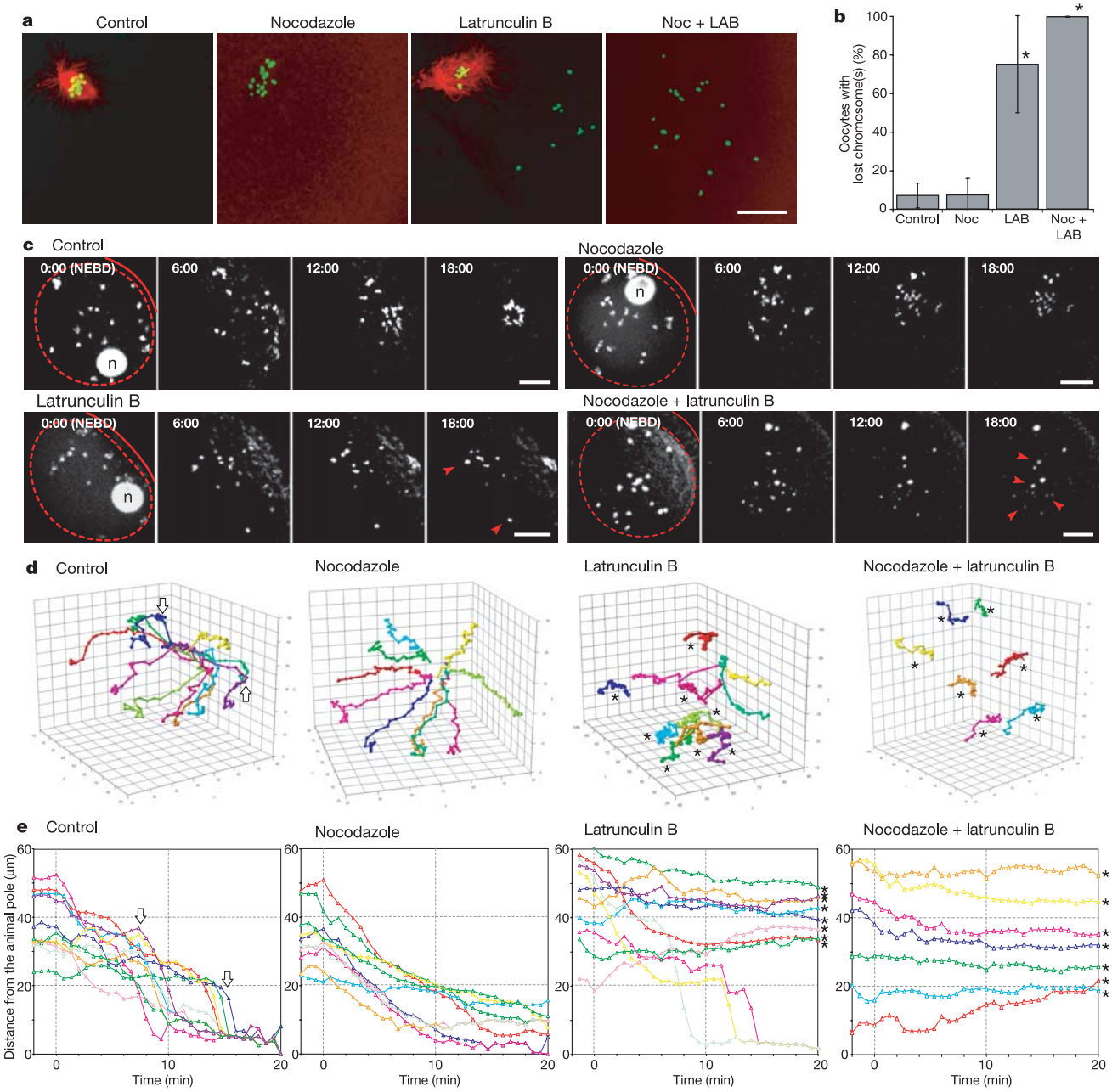

Figure 2 | Chromosome congression is independent of microtubules but relies on actin polymerization. a, Immunofluorescence of oocytes matured without treatment or in 3.3 μM nocodazole (Noc), 250 nM latrunculin B (LAB) or a combination of both. *Z*-projections of oocytes fixed 30 min after NEBD. Microtubules shown in red, DNA in green. Scale bar, 20 μm. **b**, Batches of oocytes were fixed 30 min after NEBD, stained for DNA and scored for the presence of all chromosomes at the animal pole. Averages and standard deviations from four independent experiments are shown ($n \geq 50$ each). Asterisks mark significant differences from control oocytes ($P < 0.05$, Student's *t*-test). Variations originate mainly as a result of differences in the ages of animals. **c**, 4D imaging of chromosomes in live oocytes (20 slices every 3 μm, image stacks taken every 40 s), showing *Z*-projections of selected time points. Solid line, cortex; dashed line, nucleus; n, nucleolus (disassembling shortly after NEBD). Red arrowheads show examples of lost chromosomes. Oocytes treated with nocodazole were pre-incubated for 1 h and matured in 3.3 μM nocodazole. For oocytes treated with latrunculin B, 2 μM latrunculin B was added 10 min before NEBD. For treatment with both nocodazole and latrunculin B, oocytes were matured in 3.3 μM nocodazole and 250 nM latrunculin B. Chromosomes were labelled by expressing H2B–diHcRed (which also labels the nucleolus) or by injecting Alexa-568-Ran (nocodazole + latrunculin B). Time shown in minutes and seconds. Scale bar, 20 μm. Full videos, reconstructions and tracking are available in Supplementary Videos S2–S5. **d**, 3D chromosome tracks for the data sets shown in **c**. **e**, Distances of chromosomes from the animal pole over time, calculated from **d**. Corrected for translational movement of the oocyte. Arrows in **d** and **e** highlight coinciding changes in speed and direction; lost chromosomes are labelled with asterisks. A high dose (2 μM) of latrunculin B caused rotation of the cell cortex at late times, distorting tracks of chromosomes close to the cell surface (for example, red, yellow and pale green tracks).

polymerization could not be induced by perforating the nucleus with a microneedle, by injecting phalloidin into oocyte nuclei or by overexpressing green fluorescent protein (GFP)-labelled actin artificially targeted to the nucleus by a nuclear localization signal (not shown), indicating that M-phase progression is required for actin polymerization in the nuclear region.

In contrast, exactly correlated in space and time with NEBD, we observed massive actin polymerization at the nuclear rim, which electron microscopy revealed to be directly underneath the nuclear envelope (Fig. 3c, d). The polymerization wave initiated 30–60 s before the fragmentation of nuclear membranes (visualized by the entry of a 160-kDa fluorescent dextran[14]) and also depleted the soluble nuclear actin pool (Fig. 3a, b). At this stage, nuclear pore complexes are largely disassembled and the nuclear envelope is permeable to smaller dextrans similar in size to actin as well as proteins up to several hundred kDa (Fig. 3a, b and ref. 14). We therefore conclude that after M-phase progression has been initiated, it is simply the mixing of nuclear and cytoplasmic compartments caused by NEBD that induces actin polymerization. That actin polymerization is a consequence, rather than a cause of NEBD, is also indicated by the fact that latrunculin B treatment did not affect NEBD (not shown).

An F-actin network moves chromosomes

The initial actin polymerization at the site of nuclear envelope disruption rapidly extended to a shell engulfing the entire nucleus (Figs 3a and 4a). The actin shell then depolymerized again within 1–2 min except for dense actin patches around chromosomes (Fig. 4a, b). We could observe filaments connecting these patches, but the contrast was low owing to the large soluble pool of fluorescent G-actin. To specifically detect polymerized actin we expressed an enhanced (E)GFP-tagged F-actin-binding domain of the actin-binding protein ABP-120 (EGFP–ABD, ref. 19). This enabled us to clearly visualize a network of actin filaments in the nucleoplasmic region connecting the patches around chromosomes (Fig. 4b, c and Supplementary Videos S6, S7). We confirmed identical structures by staining with phalloidin in fixed oocytes (Fig. 4e and also seen in part earlier, ref. 20) or by microinjecting phalloidin into live oocytes (Fig. 4f). High resolution time-lapse imaging of EGFP–ABD showed that contraction of the actin network delivered embedded chromosomes to the animal pole (Supplementary Videos S6, S7). The actin patches persisted around chromosomes during the low speed motion (Fig. 4d), and disappearance of the patch was shortly followed by fast microtubule capture (Fig. 4d and Supplementary Video S6). This provides a direct explanation for the actin-dependent phase of

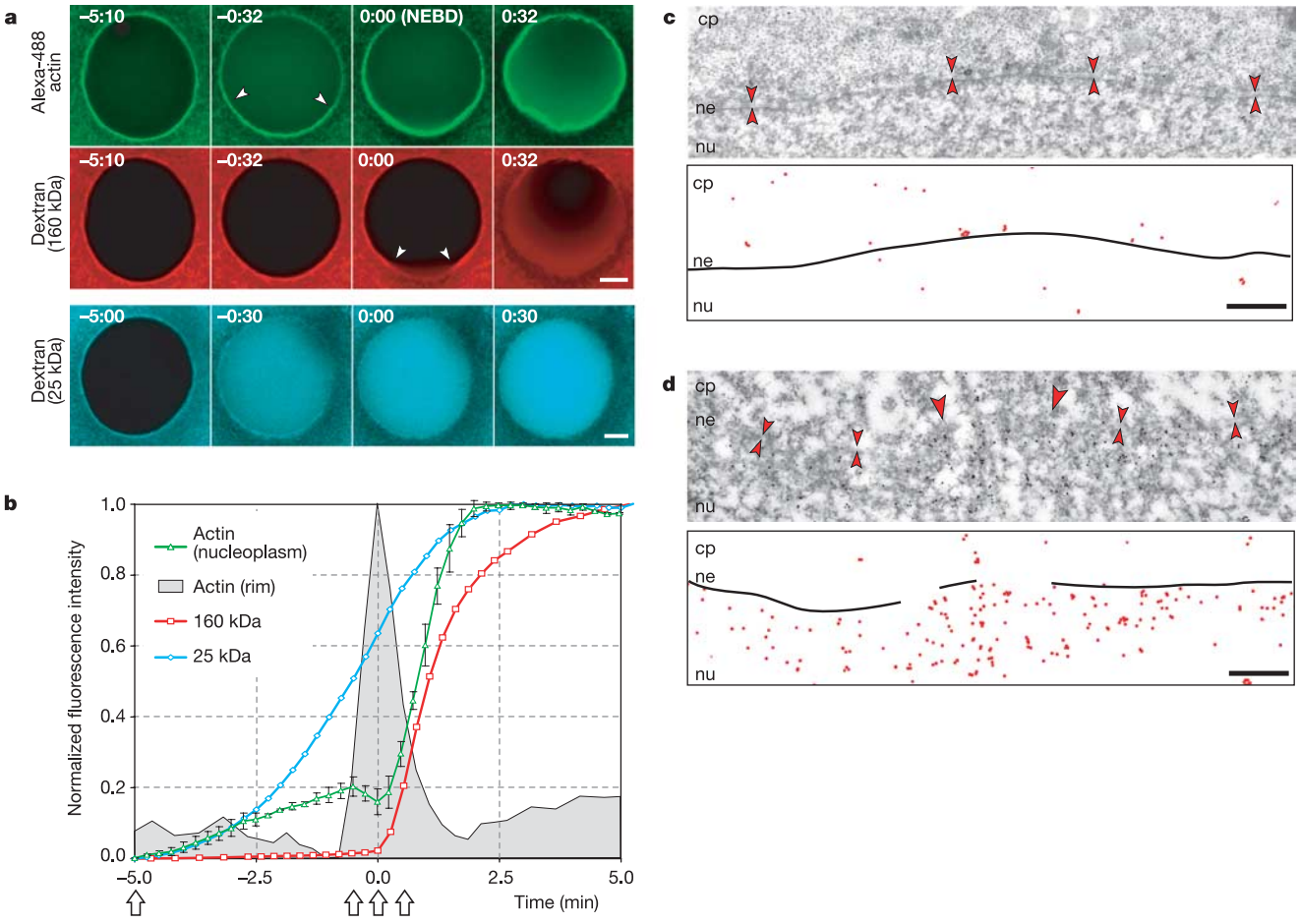

Figure 3 | Actin polymerization initiates at NEBD. **a**, Oocytes injected with Alexa-488-actin and 160 or 25 kDa TRITC-labelled dextran. Shown are single optical sections along the equator of the nucleus. Sequences were aligned to the initiation of the actin wave. The actin channel is omitted for the 25 kDa data set. Arrowheads denote region of initial actin polymerization or dextran entry. Time shown in minutes and seconds. Scale bar, 20 μm. **b**, Quantification of **a**, showing entry kinetics of actin and dextran as mean fluorescence intensities in the nuclear region (for actin average and standard deviation of the 160 and 25 kDa experiments). The nuclear rim was also quantified for actin polymerization. Data were normalized from minimum to maximum values. Arrows mark time points shown in **a**. **c**, **d**, Electron micrographs of immunogold labelling with an anti-actin antibody on a thin section fixed before (**c**) or at the time of (**d**) NEBD. Double arrowheads mark the nuclear envelope; cp, cytoplasm; ne, nuclear envelope; nu, nucleus. Scale bar, 1 μm. Schematics show gold particles and an outline of the nuclear envelope. Single arrowheads in **d** mark nuclear envelope fragments after fenestration of the nuclear envelope[14].

chromosome congression. Furthermore, beads coated with plasmid DNA injected into oocyte nuclei triggered the formation of actin patches similar to chromosomes but empty beads had no effect, indicating a chromatin-specific mechanism of actin nucleation (Fig. 4g, Supplementary Fig. S3 and Supplementary Videos S10, S11).

Depolymerization is required for contraction

Using any of the methods of visualization, the F-actin network collapsed towards the animal pole over time, suggesting that either bundling of filaments or depolymerization could drive its contraction. To test the latter hypothesis, we examined the effect of two drugs (phalloidin and jasplakinolide) that stabilize actin filaments[21]. Cells treated with either of the compounds showed severe chromosome loss, similar to latrunculin B (Fig. 5a, b). Importantly, both phalloidin and jasplakinolide were also effective if applied after NEBD, indicating that stabilization of actin filaments can prevent contraction of the already formed network (Fig. 5a, b). In control cells, the network completely depolymerized in less than 10 min (Fig. 4b and Supplementary Videos S6, S7). In contrast, in cells injected with rhodamine-phalloidin, the network was still largely intact even 20 min after NEBD (Fig. 5b and Supplementary Video S8). Thus, actin depolymerization is required for contraction of the network. Moreover, time-lapse imaging of the filament network (Supplementary Video S7) revealed streaming of thin filaments towards the animal pole. We therefore propose that the directionality of the contraction could be due to a local depolymerization of actin around the centrosomes and/or anchoring of the nuclear actin network to the cell cortex at the animal pole[22]. This would result in a 'fishnet' like mechanism, in which the three-dimensional actin net is 'pulled in' from the animal pole, carrying with it the attached chromosomes.

Although we could not observe filament thickening by live imaging of the actin network (Supplementary Video S7), we cannot rule out that myosin II-driven bundling contributes to the contraction, as it has been reported in morphologically similar actin filament networks in *Xenopus* egg extracts[23]. In such a model, the nucleoplasm of starfish oocytes could behave in a manner similar to

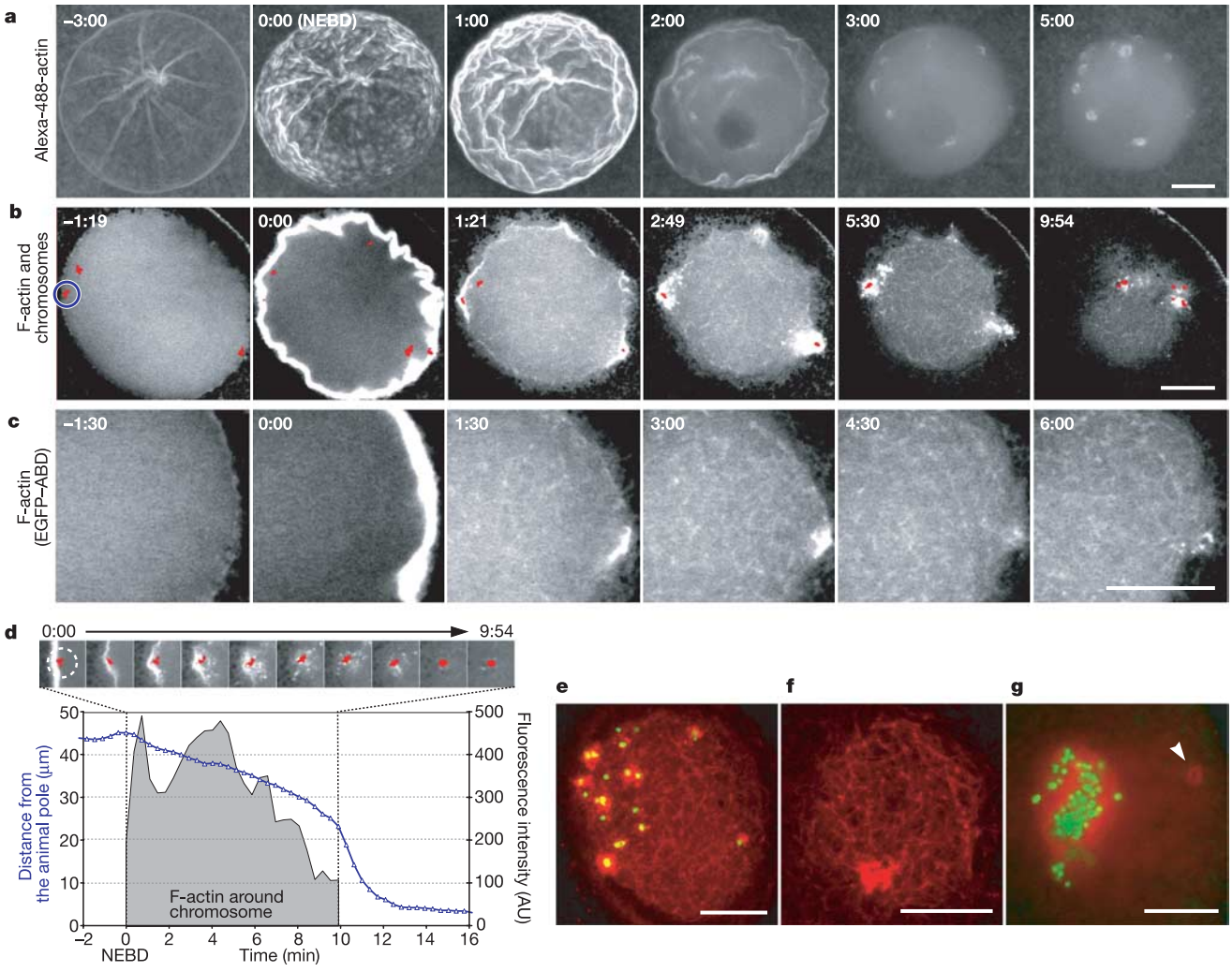

Figure 4 | Actin polymerizes into a contractile network in the nuclear region that moves chromosomes to the animal pole. **a**, 4D imaging of a maturing oocyte injected with Alexa-488-actin (15 sections every 2.75 μm, image stacks taken every 60 s), showing *Z*-projections of selected time points. **b**, 4D imaging of an oocyte expressing EGFP–ABD (F-actin, grey) injected with Alexa-568-Ran (chromosomes, red) (3 sections every 3.8 μm, image stacks every 22 s). Images show single confocal sections at selected time points. See Supplementary Video S6 for a full video. **c**, Enlarged region of an oocyte nucleus expressing EGFP–ABD, showing details of the actin network. Images show single confocal sections. See Supplementary Video S7 for a full video. **d**, Quantification of the chromosome circled in blue in **b**. Distance from animal pole (blue line) and mean EGFP–ABD fluorescence intensity (grey shading) over time. **e**, *Z*-projection of an oocyte fixed 5 min after NEBD, showing F-actin (TMR-phalloidin) staining in red and DNA in green. **f**, Single confocal section showing TMR-phalloidin injected into a live oocyte 5 min after NEBD. **g**, DNA-coated beads (green) were microinjected into the nucleus and the oocyte was imaged during maturation. Actin (Alexa-488-actin, red) forms patches around beads similar to chromosomes. Arrowhead shows an actin patch around a chromosome. Time shown in minutes and seconds (**a**–**d**). Scale bar, 20 μm.

in vitro-formed contractile actomyosin gels[24,25]. If such a gel were anchored to the animal pole, myosin-driven contraction could also provide the observed directionality. We attempted to test a role for myosin II by treating oocytes with blebbistatin, a specific inhibitor of myosin II or the Rho-associated protein kinase inhibitor Y-27632. Although neither compound affected chromosome congression, they failed to block myosin II-dependent polar body extrusion (not shown), making these experiments inconclusive.

Actin dependence in oocytes of other species

In summary, we have shown that in starfish oocytes, microtubules alone are unable to capture chromosomes more than 40 μm away from centrosomes. Instead, an actin 'fishnet' is essential for delivering chromosomes within the capture distance of microtubule asters. A similar architectural problem exists in many animal species, as oocytes have large nuclei for storing nuclear proteins and RNA. For example, *Xenopus* oocytes are morphologically similar to those of starfish and contain a microtubule array of 50–80-μm radius that has to capture chromosomes in a 500-μm diameter nucleus[26]. Consistent with our observations, disrupting the actin cytoskeleton with cytochalasin B has been reported to cause defects in spindle formation in *Xenopus* oocytes[27,28]. Moreover, in meiosis I of mouse oocytes, chromosomes are known to move to the cell cortex in an actin-dependent manner, even in the absence of microtubules[29–31]. This strongly suggests that actin nucleation on M-phase chromatin, which we directly visualized for the first time in starfish oocytes, is an evolutionarily conserved mechanism that is also functional in vertebrates and mammals. In starfish oocytes, failure of actin-dependent chromosome congression did not delay anaphase and consequently led to chromosome loss and aneuploidy. Such failure should have similar deleterious effects in *Xenopus* oocytes, because the spindle checkpoint is inactive in meiosis I (ref. 32), and although the checkpoint is active in mouse, oocytes escape checkpoint arrest after few hours[33]. At least 5% of human oocytes are aneuploid, and aneuploidy is the leading cause of pregnancy loss and birth defects[34]. It will therefore be important to test whether a similar actin-dependent mechanism is also involved in chromosome congression in humans.

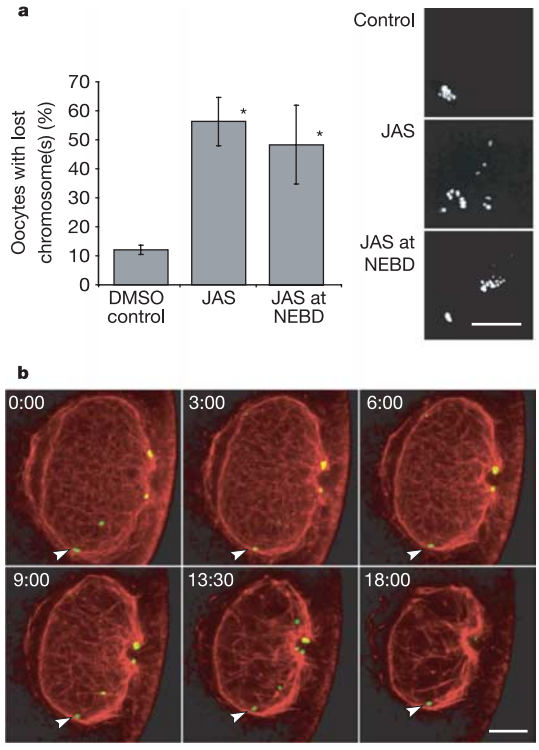

Figure 5 | F-actin-stabilizing drugs prevent chromosome movement and contraction of the actin network. a, Oocytes were matured in 0.1% DMSO or 1 μM jasplakinolide (JAS+0.01% DMSO), or 10 μM JAS (+0.1% DMSO) was added 2 min after NEBD. Oocytes were fixed 30 min after NEBD, stained for DNA and scored for the presence of all chromosomes at the animal pole. Data show average ± s.d. from two independent experiments ($n \geq 50$ each). Asterisks mark significant differences from control oocytes ($P < 0.05$, Student's *t*-test). **b**, 4D imaging of an oocyte expressing H2B–EGFP (green) and injected with TMR-phalloidin (red) approximately 3 min after NEBD (25 sections every 2.75 μm, image stacks taken every 45 s). Single confocal sections of selected time points are shown; see Supplementary Video S8 for a full video. Arrowhead indicates a lost chromosome. Time shown in minutes and seconds. Scale bar, 20 μm (**a**, **b**).

METHODS

Oocyte injection, maturation and drug treatments. Starfish (*Asterina miniata*) were obtained from Marinus Scientific and maintained as described in ref. 14. Oocytes were isolated and injected with mercury-filled needles using methods described elsewhere (ref. 14; see also http://155.37.3.143/panda/injection/index.html). Injection and microscopy were done at 20 °C. mRNA-injected oocytes were incubated overnight at 16 °C, or in the case of H2B–DiHcRed-expressing oocytes, for 36 h to allow incorporation of core histones. Maturation was triggered by the addition of 1–10 μM 1-methyladenine (Sigma). NEBD typically started 20 min after hormone addition, and only oocytes starting NEBD between 15 and 35 min were analysed.

For drug treatments, oocytes were matured in 3.3 μM nocodazole or 250 nM latrunculin B (both from EMD Biosciences, diluted from 1 mg ml^{-1} stocks), which efficiently depolymerized microtubules and actin filaments, respectively (Supplementary Fig. S1). In some cases, oocytes were also preincubated with the drugs for 30 min before maturation, which gave identical results. In live-cell imaging experiments, latrunculin B was added at 100–2,000 nM concentrations 10 min after hormone addition to prevent shape changes of oocytes caused by disruption of cortical actin. Jasplakinolide (Molecular Probes) was dissolved at 0.7 mg ml^{-1} in dimethylsulphoxide (DMSO) and used at a final concentration of 1 or 10 μM.

GFP constructs and fluorescent markers. H2B–DiHcRed[16], ensconsin–3EGFP (3EGFP–EMTB)[35] and EGFP–ABD[19] were transferred from constructs for mammalian expression to pGEMHE for *in vitro* transcription as described in ref. 14. Capped mRNA was synthesized from linearized templates using the mMessage mMachine kit (Ambion), dissolved in 10 μl water (typically 1–2 μg μl^{-1}) and injected to 1–5% oocyte volume.

Alexa-488-labelled rabbit muscle actin (Molecular Probes; 11 mg ml^{-1}) was diluted 1:4 in G-buffer (2 mM Tris pH 8.0, 0.1 mM ATP, 0.1 mM dithiothreitol, 0.1 mM $CaCl_2$) and injected to 5% oocyte volume. In some experiments, Alexa-488- or Alexa-568-labelled Ran was used to label chromosomes[36]. From the concentrated stocks (50 and 60 μM, respectively), amounts corresponding to 0.5–1% of the egg volume (2–5% of the endogenous Ran protein level[36]) were injected. To inject rhodamine-phalloidin (Molecular Probes), 50 μl of methanol stock was dried, dissolved in 1 μl water and injected into oocytes.

DNA-coated beads were prepared as previously published[37], except that DNA was fluorescently labelled by incorporating Cy3-dUTP (Amersham) and 1-μm diameter beads (Dynabeads MyOne Streptavidin, Dynal Biotech) were used.

Immunofluorescence. We have used the methods developed in ref. 38, with minor modifications. Briefly, oocytes were fixed in buffer containing 100 mM HEPES buffer, 50 mM EGTA, 10 mM $MgSO_4$, 2–500 mM maltose, 2% formaldehyde, 0.2% glutaraldehyde and 0.2% Triton-X100 for 2 h at 20 °C. Oocytes were extracted overnight in 0.2% Triton-X100 in PBS, blocked with PBS + 5% BSA and incubated with a monoclonal anti-α-tubulin antibody (DM 1A, Sigma) and Alexa-488-labelled secondary antibody (Molecular Probes). Rhodamine-phalloidin was from Molecular Probes, the methanol stock was dried then dissolved in PBS, and oocytes were stained for 1 h at 20 °C. DNA was stained by incubating oocytes for 1 h with 5 μg ml^{-1} Hoechst 33342 (Molecular Probes).

Confocal microscopy and image quantification. Microscopy was done either with a customized Zeiss LSM510 Axiovert confocal microscope as described[14], using an ×40 C-Apochromat 1.2 NA water immersion objective lens (Zeiss) (Figs 1b, 2a, 3a, 4a, e–g, 5b); a Nikon C1 E-800 confocal microscope with a ×20 SuperFluar 0.7 NA dry lens (Fig. 2c–e) or a Leica TCS SP2 confocal microscope equipped with an HCX Plan Apochromat λBlue 1.2 NA ×63 water immersion objective lens (Figs 1a and 4b, c).

Time series were analysed using LSM510 software (Zeiss) and ImageJ (http://rsb.info.nih.gov/ij/). Figures were assembled using Adobe Photoshop and Illustrator. A gaussian blur filter (0.3–1 pixel) was generally applied to reduce shot noise. Three-dimensional (3D) reconstructions and tracking were done

with in-house developed software, Tikal[39]. Images were filtered using an anisotropic diffusion filter and thresholded. Binary images were reconstructed in three dimensions by isosurface rendering, and chromosomes were tracked manually. Tracks were analysed using the graphing software Excel (Microsoft) and Graphis (Kylebank Software). For rendering Fig. 1b, Amira 2.3 (TGS) was used.

Electron microscopy. Oocytes were fixed in 2% formaldehyde plus 0.2–0.5% glutaraldehyde in sea water for 2 h, then stored at 4 °C in 1% formaldehyde in sea water. After embedding in agarose, oocytes were dehydrated in cold methanol and embedded in LR Gold resin (Polysciences) at −20 °C. The LR Gold was polymerized under ultraviolet light at −20 °C. Thin sections were collected on Formvar-coated nickel grids and immunolabelled as previously described[40]. A mouse monoclonal antibody against actin (clone C4, Boehringer Mannheim) was used at a dilution of 1:10 or 1:20. Goat anti-mouse IgG labelled with 10 nm gold was obtained from Amersham Biosciences and used at a dilution of 1:20. After labelling, the sections were stained and examined under a transmission electron microscope (CM-10, Philips).

Received 22 February; accepted 3 May 2005.
Published online 13 July 2005.

1. Gadde, S. & Heald, R. Mechanisms and molecules of the mitotic spindle. *Curr. Biol.* **14,** R797–R805 (2004).
2. Rusan, N. M., Fagerstrom, C. J., Yvon, A. M. & Wadsworth, P. Cell cycle-dependent changes in microtubule dynamics in living cells expressing green fluorescent protein-α tubulin. *Mol. Biol. Cell* **12,** 971–980 (2001).
3. Zhai, Y., Kronebusch, P. J., Simon, P. M. & Borisy, G. G. Microtubule dynamics at the G2/M transition: abrupt breakdown of cytoplasmic microtubules at nuclear envelope breakdown and implications for spindle morphogenesis. *J. Cell Biol.* **135,** 201–214 (1996).
4. Kirschner, M. & Mitchison, T. Beyond self-assembly: from microtubules to morphogenesis. *Cell* **45,** 329–342 (1986).
5. Kline-Smith, S. L. & Walczak, C. E. Mitotic spindle assembly and chromosome segregation: refocusing on microtubule dynamics. *Mol. Cell* **15,** 317–327 (2004).
6. Holy, T. E. & Leibler, S. Dynamic instability of microtubules as an efficient way to search in space. *Proc. Natl Acad. Sci. USA* **91,** 5682–5685 (1994).
7. Belmont, L. D., Hyman, A. A., Sawin, K. E. & Mitchison, T. J. Real-time visualization of cell cycle-dependent changes in microtubule dynamics in cytoplasmic extracts. *Cell* **62,** 579–589 (1990).
8. Piehl, M. & Cassimeris, L. Organization and dynamics of growing microtubule plus ends during early mitosis. *Mol. Biol. Cell* **14,** 916–925 (2003).
9. Rieder, C. L. & Alexander, S. P. Kinetochores are transported poleward along a single astral microtubule during chromosome attachment to the spindle in newt lung cells. *J. Cell Biol.* **110,** 81–95 (1990).
10. Carazo-Salas, R. E. & Karsenti, E. Long-range communication between chromatin and microtubules in *Xenopus* egg extracts. *Curr. Biol.* **13,** 1728–1733 (2003).
11. Tulu, U. S., Rusan, N. M. & Wadsworth, P. Peripheral, non-centrosome-associated microtubules contribute to spindle formation in centrosome-containing cells. *Curr. Biol.* **13,** 1894–1899 (2003).
12. Wollman, R. *et al.* Efficient chromosome capture requires a bias in the 'search-and-capture' process during mitotic-spindle assembly. *Curr. Biol.* **15,** 828–832 (2005).
13. Zhang, Q. Y., Tamura, M., Uetake, Y., Washitani-Nemoto, S. & Nemoto, S. Regulation of the paternal inheritance of centrosomes in starfish zygotes. *Dev. Biol.* **266,** 190–200 (2004).
14. Lenart, P. *et al.* Nuclear envelope breakdown in starfish oocytes proceeds by partial NPC disassembly followed by a rapidly spreading fenestration of nuclear membranes. *J. Cell Biol.* **160,** 1055–1068 (2003).
15. Miyazaki, A., Kamitsubo, E. & Nemoto, S. I. Premeiotic aster as a device to anchor the germinal vesicle to the cell surface of the presumptive animal pole in starfish oocytes. *Dev. Biol.* **218,** 161–171 (2000).
16. Gerlich, D. *et al.* Global chromosome positions are transmitted through mitosis in mammalian cells. *Cell* **112,** 751–764 (2003).
17. Stricker, S. A. & Schatten, G. The cytoskeleton and nuclear disassembly during germinal vesicle breakdown in starfish oocytes. *Dev. Growth Differ.* **33,** 163–171 (1991).
18. Terasaki, M. Redistribution of cytoplasmic components during germinal vesicle breakdown in starfish oocytes. *J. Cell Sci.* **107,** 1797–1805 (1994).
19. Pang, K. M., Lee, E. & Knecht, D. A. Use of a fusion protein between GFP and an actin-binding domain to visualize transient filamentous-actin structures. *Curr. Biol.* **8,** 405–408 (1998).
20. Heil-Chapdelaine, R. A. & Otto, J. J. Characterization of changes in F-actin during maturation of starfish oocytes. *Dev. Biol.* **177,** 204–216 (1996).
21. Visegradi, B., Lorinczy, D., Hild, G., Somogyi, B. & Nyitrai, M. The effect of phalloidin and jasplakinolide on the flexibility and thermal stability of actin filaments. *FEBS Lett.* **565,** 163–166 (2004).
22. Weber, K. L., Sokac, A. M., Berg, J. S., Cheney, R. E. & Bement, W. M. A microtubule-binding myosin required for nuclear anchoring and spindle assembly. *Nature* **431,** 325–329 (2004).
23. Waterman-Storer, C. *et al.* Microtubules remodel actomyosin networks in *Xenopus* egg extracts via two mechanisms of F-actin transport. *J. Cell Biol.* **150,** 361–376 (2000).
24. Szent-Gyorgyi, A. *Chemistry of Muscular Contraction* (Academic, New York, 1951).
25. Spicer, S. S. The clearing response of actomyosin to adenosinetriphosphate. *J. Biol. Chem.* **199,** 289–300 (1952).
26. Gard, D. L. Microtubule organization during maturation of *Xenopus* oocytes: assembly and rotation of the meiotic spindles. *Dev. Biol.* **151,** 516–530 (1992).
27. Ryabova, L. V., Betina, M. I. & Vassetzky, S. G. Influence of cytochalasin B on oocyte maturation in *Xenopus laevis*. *Cell Differ.* **19,** 89–96 (1986).
28. Gard, D. L., Cha, B. J. & Roeder, A. D. F-actin is required for spindle anchoring and rotation in *Xenopus* oocytes: a re-examination of the effects of cytochalasin B on oocyte maturation. *Zygote* **3,** 17–26 (1995).
29. Longo, F. J. & Chen, D. Y. Development of cortical polarity in mouse eggs: involvement of the meiotic apparatus. *Dev. Biol.* **107,** 382–394 (1985).
30. Leader, B. *et al.* Formin-2, polyploidy, hypofertility and positioning of the meiotic spindle in mouse oocytes. *Nature Cell Biol.* **4,** 921–928 (2002).
31. Maro, B. & Verlhac, M. H. Polar body formation: new rules for asymmetric divisions. *Nature Cell Biol.* **4,** E281–E283 (2002).
32. Peter, M. *et al.* The APC is dispensable for first meiotic anaphase in *Xenopus* oocytes. *Nature Cell Biol.* **3,** 83–87 (2001).
33. Wassmann, K., Niault, T. & Maro, B. Metaphase I arrest upon activation of the Mad2-dependent spindle checkpoint in mouse oocytes. *Curr. Biol.* **13,** 1596–1608 (2003).
34. Hassold, T. & Hunt, P. To err (meiotically) is human: the genesis of human aneuploidy. *Nature Rev. Genet.* **2,** 280–291 (2001).
35. Faire, K. *et al.* E-MAP-115 (ensconsin) associates dynamically with microtubules *in vivo* and is not a physiological modulator of microtubule dynamics. *J. Cell Sci.* **112,** 4243–4255 (1999).
36. Hinkle, B. *et al.* Chromosomal association of Ran during meiotic and mitotic divisions. *J. Cell Sci.* **115,** 4685–4693 (2002).
37. Heald, R. *et al.* Self-organization of microtubules into bipolar spindles around artificial chromosomes in *Xenopus* egg extracts. *Nature* **382,** 420–425 (1996).
38. Strickland, L. *et al.* Light microscopy of echinoderm embryos. *Methods Cell Biol.* **74,** 371–409 (2004).
39. Bacher, C. P., Reichenzeller, M., Athale, C., Herrmann, H. & Eils, R. 4-D single particle tracking of synthetic and proteinaceous microspheres reveals preferential movement of nuclear particles along chromatin-poor tracks. *BMC Cell Biol.* **5,** 45 (2004).
40. Hand, A. R. in *Introduction to Biophysical Methods for Protein and Nucleic Acid Research* (eds Glasel, J. & Deutscher, M.) 205–260 (Academic, New York, 1995).

Supplementary Information is linked to the online version of the paper at www.nature.com/nature.

Acknowledgements Part of this work was performed at the Marine Biological Laboratory (MBL) in Woods Hole, supported by summer research fellowships from Nikon Inc. and the E. and M. Spiegel, F.B. and B.G. Bang, L.B. Lehmann, R.D. Allen and H.W. Rand foundations to J.E. Martin Hoppe and Leica Microsystems in Mannheim are gratefully acknowledged for providing equipment at the MBL. P.L. was supported by a predoctoral fellowship from the Louis-Jeantet Foundation. We would like to thank J. C. Bulinski for providing p3EGFP-EMTB, K. Weijer for EGFP-ABD and K. Ribbeck for fluorescently labelled Ran.

Author Information Reprints and permissions information is available at npg.nature.com/reprintsandpermissions. The authors declare no competing financial interests. Correspondence and requests for materials should be addressed to J.E. (jan.ellenberg@embl.de).